Anatase TiO 2 Nanorods as Cathode Materials for Aluminum-Ion Batteries

Shutao Wang, Kostiantyn Kravchyk, Stéphanie Pigeot-Remy, Weiqiang Tang, Frank Krumeich, Michael Wörle, Maryna I Bodnarchuk, Sophie Cassaignon, Olivier Durupthy, Shuangliang Zhao, et al.

Anatase TiO_2 Nanorods as Cathode Materials for Aluminum-Ion Batteries

Shutao Wang,[1,2,#] Kostiantyn V. Kravchyk,[1,2,#] Stephanie Pigeot-Rémy,[3] Weiqiang Tang,[4] Frank Krumeich,[1] Michael Wörle,[1] Maryna I. Bodnarchuk,[2] Sophie Cassaignon,[3] Olivier Durupthy,[3] Shuangliang Zhao,[4] Clément Sanchez,[3] and Maksym V. Kovalenko[,1,2]*

[1] Laboratory of Inorganic Chemistry, Department of Chemistry and Applied Biosciences, ETH Zürich, Vladimir-Prelog-Weg 1, CH-8093 Zürich, Switzerland

[2] Laboratory for Thin Films and Photovoltaics, Empa – Swiss Federal Laboratories for Materials Science and Technology, Überlandstrasse 129, CH-8600 Dübendorf, Switzerland

[3] Sorbonne University, CNRS, College of France, PSL Research University, Laboratory Chemistry of the Condensed Matter of Paris, LCMCP, 4 Place Jussieu, F-75005 Paris, France

[4] State Key Laboratory of Chemical Engineering and School of Chemical Engineering, East China University of Science and Technology, 200237, Shanghai, China

[#]Equal contributions

Corresponding Author

*E-mail: mvkovalenko@ethz.ch

KEYWORDS: Al-ion battery, aluminum, titanium (IV) oxide, energy storage, nanorod, synthesis.

ABSTRACT

In view of the practical deployment of Al-ion batteries for stationary energy storage, novel and cost-efficient cathodes consisting of earth-abundant chemical elements are imperative. Titanium dioxide TiO_2 is an appealing candidate as a cathode material due to high natural reserves of the constituent elements as well as its nontoxicity and high chemical robustness. In this work, we assessed the potential of anatase TiO_2 nanorods as a cathode material for Al-ion storage. This material delivers high capacities of 112-165 mAh g^{-1} at a current density of 50 mA g^{-1} in $AlCl_3$/1-Ethyl-3-methylimidazolium chloride ionic liquid electrolyte of various acidity. The mechanism of aluminum intercalation into anatase TiO_2 nanorods and the related crystal structure changes were assessed by density functional theory, *ex situ* X-ray photoelectron and energy-dispersive X-ray spectroscopies.

INTRODUCTION

Al-ion batteries (AIBs) are appealing as an inexpensive electrochemical energy storage technology and have attracted significant attention in the last few years.[1-2] Aluminum has numerous advantages such as high natural abundance, high volumetric/gravimetric (8046 mAh cm^{-3}/2980 mAh g^{-1}) capacities and low redox potential.[3-8] Contrary to metallic Li, Na, and K, Al could be utilized in the form of metallic foil on the anode part of the battery due to smooth and fast electrodeposition/stripping. Thus far, the main barrier for the progress of AIBs has been the scarcity of cathodes supporting Al^{3+} ion intercalation/deintercalation. In this arena, an important difference exists in comparison to univalent Li^+/Na^+ cations. Intercalation of Al^{3+} cations, being much smaller than Li^+ ions, was revealed to be difficult as a result of strong Coulombic interaction with the lattice of the host cathode material.[9] In the last few years, various materials have been explored with respect to Al^{3+} ion storage, such as transition metal oxides,[10-22] sulfides,[23-36] selenides,[37-38] phosphite,[39] molybdite,[40] vanadate,[41] carbide,[42] Prussian blue analogs,[43-44] iodine,[45] selenium,[46] sulfur[47-49] and oxygen.[50] Overall, the reversibility of the Al^{3+} ion intercalation/deintercalation redox processes has been demonstrated, although nearly all known cathodes possess poor rate capabilities and limited cycle life.

Of all possible cathode materials for AIBs, titanium oxide (TiO_2) is probably the most appealing candidate due to high natural reserves of the constituent elements, its nontoxicity, and high oxidation stability. Reversible intercalation of Al^{3+} ions into TiO_2 was first demonstrated in 2012 by Liu *et al.*[16] on anatase TiO_2 nanotube arrays in an aqueous $AlCl_3$ electrolyte. The reduction of Ti^{4+} to Ti^{3+}/Ti^{2+} during Al^{3+} ion intercalation has been confirmed by XPS studies. Later, reversible Al^{3+} ion storage was shown on anatase TiO_2 nanospheres.[51] Despite these achievements, Al^{3+} ion intercalation in TiO_2 has been reported up to recently only in aqueous electrolytes, which are, however, susceptible to parasitic reactions such as chemical oxidation of the aluminum anode and hydrogen evolution during aluminum

deposition. In the context of minimization of these side reactions, Koketsu *et al.*[19] reported the electrochemical performance of cation-deficient anatase TiO_2 in a chloroaluminate ionic liquid electrolyte which demonstrated a high capacity of 120 mAh g^{-1} in comparison with pure bulk TiO_2 (30 mAh g^{-1}). However, the electrochemical performance of cation-deficient anatase TiO_2 was only reported for three cycles.

Encouraged by both the initial reports on TiO_2 in an aqueous electrolyte[16, 51-52] and the recent publications of Koketsu *et al*.,[19] and others[53] we sought to thoroughly evaluate the Al^{3+} ion storage performance of nanosized anatase TiO_2 in chloroaluminate ionic liquid. Herein, we demonstrate that anatase TiO_2 nanorods (NRs) deliver a high capacity of 112 mAh g^{-1} and 165 mAh g^{-1} at a current density of 50 mA g^{-1} in mild and highly acidic formulations ($AlCl_3$/1-Ethyl-3-methylimidazolium chloride (EMIMCl) with molar ratios of 1.1:1 and 2.0:1), respectively. The mechanism of Al^{3+} ion intercalation into TiO_2 NRs in both formulations has been assessed using *ex situ* X-ray photoelectron (XPS) and energy-dispersive X-ray (EDX) spectroscopies. Density functional theory (DFT) calculations were performed to predict the volume change of the TiO_2 structure during Al^{3+} ion intercalation.

RESULTS AND DISCUSSION

In this work, monodispersed TiO_2 NRs were synthesized using a previously reported method;[54-55] briefly, the synthesis of NRs was performed by hydrothermal treatment of titanium isopropoxide in the presence of triethanolamine and ethylenediamine (see **Figure S1** and Experimental Section for details). As follows from transmission electron microscopy (TEM) measurements, TiO_2 NRs were crystalline with length and width on the average order of 50-200 nm and 7-14 nm, respectively (**Figure 1a**). As illustrated in **Figure 1b**, the powder X-ray diffraction (XRD) and selected area electron diffraction patterns of TiO_2 NRs show a tetragonal anatase structure with the space group $I4_1/amd$. The lattice parameters, as obtained from a Rietveld refinement, are: $a = b = 3.80002(10)$ Å, c = 9.5010(2) Å. Notably, in

accordance with Rietveld refinement, about 6.3% of brookite phase was present in TiO_2 NRs (see **Figure S2**, **Table S1** and Experimental Section for details). As follows from high-resolution transmission electron microscopy (HRTEM) imaging (see inset of **Figure 1b**), the growth direction of TiO_2 NRs is [001] and the top facet of TiO_2 NRs is a plane (010).

For the electrochemical tests, TiO_2 NRs were mixed with polyvinylidene fluoride (PVDF) binder, carbon black (CB), titanium nitride (TiN) and N-methylpyrrolidone (NMP). The obtained slurry was cast onto tungsten plates. A homemade plastic cell design was used for the electrochemical measurements (**Figure S3**). Aluminum ionic liquid electrolyte consisting of $AlCl_3$:EMIMCl with molar ratios of 1.1 or 2.0 was employed as an electrolyte.

Figure 1c shows the voltage profiles of the AIB at a current density of 50 mA g^{-1} using TiO_2 NRs as a cathode material. During the first discharge, the intercalation of approximately 0.12 mol of Al^{3+} ions per mole of TiO_2 was observed, which corresponds to a total initial discharge capacity of 121 mAh g^{-1}. During the first charge cycle, all inserted Al^{3+} ions could be extracted from the TiO_2 structure. The discharging half-reactions can be written as follows:

On anode: $$xAl + 7xAlCl_4^- \leftrightarrow 4xAl_2Cl_7^- + 3xe^- \quad (1)$$

On cathode: $$4xAl_2Cl_7^- + TiO_2 + 3xe^- \leftrightarrow Al_xTiO_2 + 7xAlCl_4^- \quad (2)$$

As follows from **Figures 1c** and **1d**, TiO_2 NRs showed superior electrochemical performance over bulk TiO_2. Bulk TiO_2 shows only a small capacity of 35 mAh g^{-1}, which is also in agreement with results of Koketsu *et al.*[19] Apparently, decreasing the crystal grain size of the TiO_2 shortens the ionic diffusion length and increases the active material/electrolyte interactions. Consequently, TiO_2 NRs possess significantly higher electrochemical activity as compared to micron-sized TiO_2 particles (**Figure S4**).

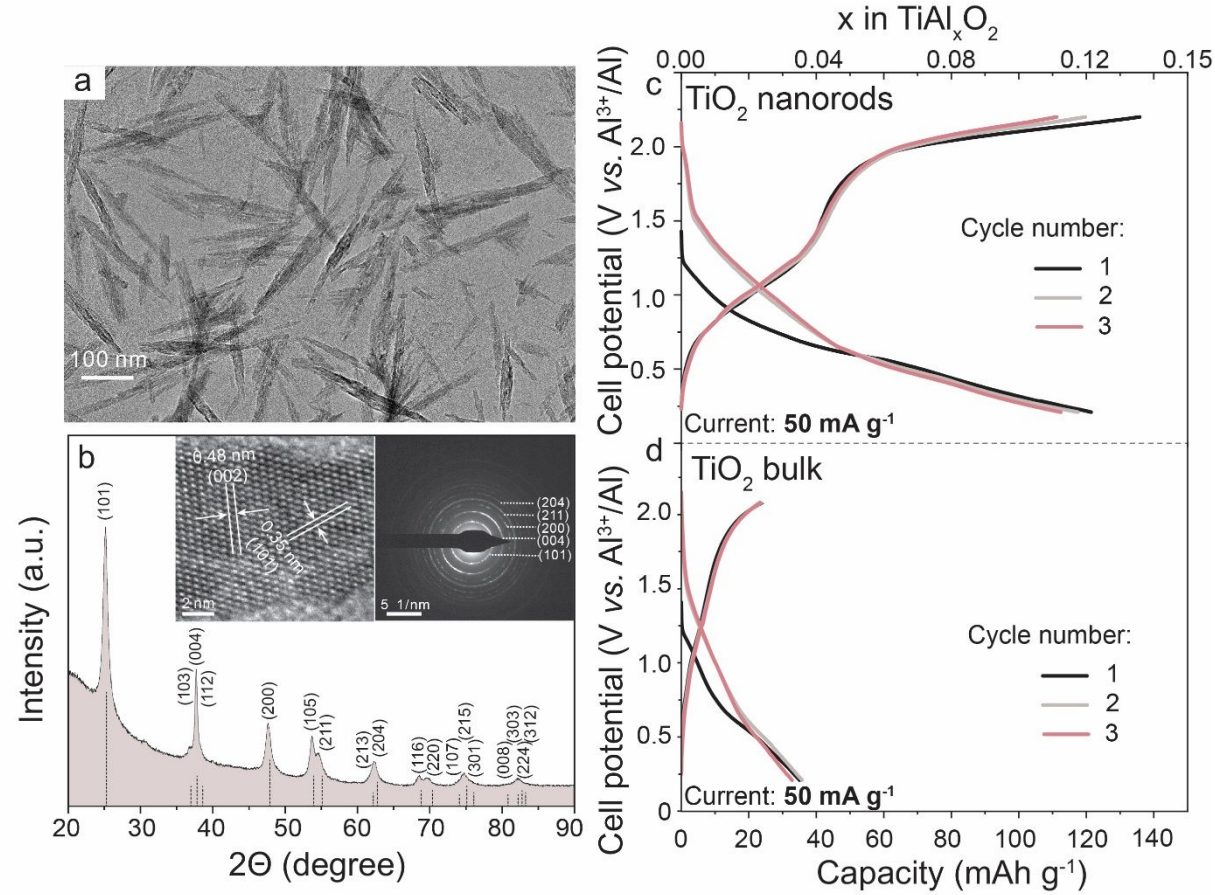

Figure 1. (a) Transmission electron microscopy (TEM) image and (b) X-ray diffraction (XRD) pattern of TiO_2 NRs [inset: high-resolution TEM image and selected area electron diffraction (SAED) image of TiO_2 NRs]. First three galvanostatic charge-discharge curves of TiO_2 NRs (c) and microcrystalline bulk TiO_2 (d) using $AlCl_3$:EMIMCl electrolytes (1.1:1 molar ratio).

Next, we compared the electrochemical behavior of TiO_2 NRs in mild and highly acidic $AlCl_3$/EMIMCl ionic liquid electrolytes with $AlCl_3$:EMIMCl molar ratios of 1.1:1 and 2.0:1 (low and high $AlCl_3$ molar fractions), respectively (**Figure 2,** see **Figure S5** for cyclic voltammetry measurements). As follows from **Figure 2**, TiO_2 NRs exhibited a higher capacity of 165 mAh g^{-1} with the higher $AlCl_3$:EMIMCl molar ratio of 2.0 compared to 112 mAh g^{-1} when using the lower molar ratio of 1.1. The detailed Al^{3+} ion charge storage mechanism for TiO_2 NRs in both mild and highly acidic $AlCl_3$/EMIMCl ionic liquid electrolytes was first interrogated by *ex situ* XPS. **Figure 2b** shows the change of Al 2p, Cl 2p, and Ti 2p XPS peaks for pristine, discharged and charged samples. For discharged electrode, at both 2.0 and 1.1 molar ratios, the Ti 2p peak displaced to higher binding energy, as a result of Ti^{4+} reduction to Ti^{3+}. Upon the following charge, Ti^{3+} is oxidized back to Ti^{4+}.

As evident from the Al 2p XPS spectra for both the 2.0 and 1.1 ratios, the Al peak appears after discharge and fully vanishes after the following charge. However, in the case of the 2.0 ratio, the Cl 2p signal was also observed for the discharged electrode, which disappeared after the following charge. Appearance of Cl was also observed on the EDX maps for the 2.0 ratio, in contrast to the 1.1 ratio (see **Figures S10** for details). The quantitative XPS analysis of the discharged TiO_2 electrode using $AlCl_3$/EMIMCl ionic liquid with 2.0 molar ratio revealed the following atomic ratios for Al and Cl: 2.5(±0.1) and 2(±0.1). We assume that the appearance of the Cl in the discharged TiO_2 electrode can be attributed to the presence of $AlCl_2^+$ species in the highly acidic $AlCl_3$:EMIMCl ionic liquid electrolyte, and this has been confirmed in a series of previous reports[56-60] as well as in the present work by solution state ^{27}Al NMR measurements (**Figure S11**). It is possible that the $AlCl_2^+$ species is too large for intercalation ($r(AlCl_2^+)$ = 3.76 Å *vs*. $r(Al^{3+})$ = 0.53 Å) and can be attracted by Coulombic forces to the reduced Ti^{3+} ion sites on the surface of the TiO_2 NRs, contributing to the aluminum charge storage mechanism. These assumptions might explain why the capacity of TiO_2 in the highly acidic electrolyte is higher than that of the mildly acidic electrolyte.

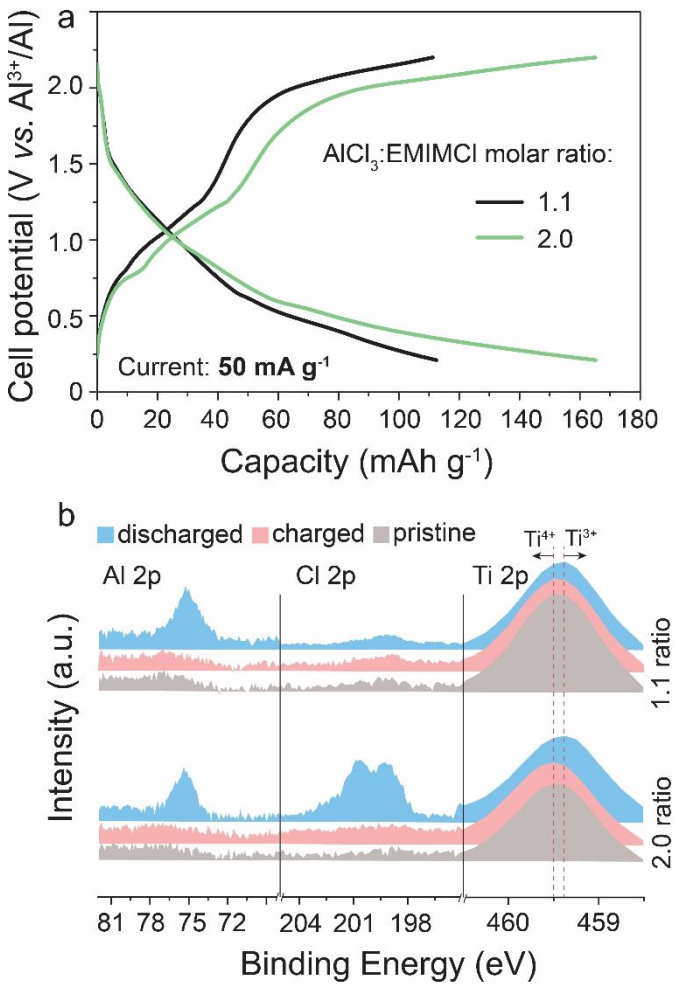

Figure 2. (a) Typical galvanostatic charge-discharge curves (3rd cycle) of TiO_2 NRs measured at a current density of 50 mA g^{-1} in mild (1.1:1 molar ratio) and acidic (2.0:0 molar ratio) $AlCl_3$/EMIMCl ionic liquid electrolytes. See **Figure S6** for the electrochemical performance of TiO_2 NRs in chloroaluminate ionic liquid with 1.1, 1.3, 1.5, and 2.0 $AlCl_3$/EMIMCl molar ratios measured at a current density of 0.5 A g^{-1}. (b) *Ex situ* XPS measurements of electrodes composed of TiO_2 NRs before and after discharge and charge in $AlCl_3$/EMIMCl ionic liquid electrolytes (1.1:1 and 2.0:0 molar ratios). See **Figures S7** and **S8** for the detailed O 1s and Ti 2p XPS spectra. Full XPS survey spectra are shown in **Figure S9**.

To better understand the structural changes during Al^{3+} ion intercalation into the anatase TiO_2 structure, DFT calculations were performed.[20] Specifically, we gradually increased the number of Al^{3+} ions in the intercalation sites of an anatase supercell and fully relaxed the supercell volume and the atomic positions of the host. We note that at low Al^{3+} ion content (the molar fraction of aluminum $x < 0.167$, and the capacity of 163 mAh g^{-1}), the repulsive force between the Al-Ti is the major factor affecting the stability of the Al^{3+} ion intercalation site. As follows from the DFT study during Al^{3+} ion intercalation into TiO_2, the anatase TiO_2

supercell is stable (see the corresponding structures of Al^{3+} ion intercalated TiO_2 at various x on **Figure 3a** and **Figure S12**). The computed relative volume change of anatase TiO_2 structure varies with the molar ratio x in Al_xTiO_2, as shown in **Figure 3b**. We found that the cell volume of the TiO_2 structure gradually increased with an increase of Al^{3+} ion content and tended to be at the highest value of 140 Å (relative volume change of 2.1%).

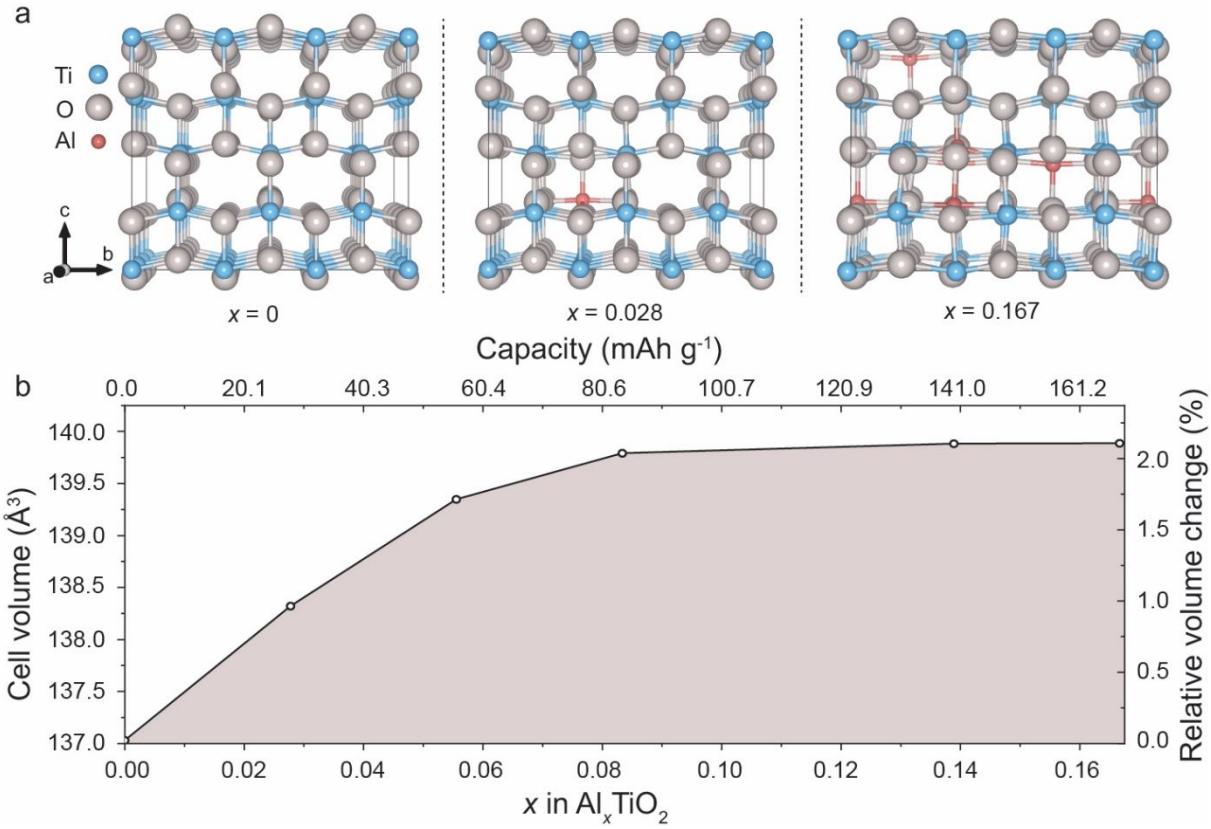

Figure 3. (a) Representation of the crystal structures of TiO_2 with different A^{3+} ion content ($x = 0$; $x = 0.028$; $x = 0.167$). Gray, blue, and red spheres represent O, Ti, and Al atoms, respectively. (b) The dependence of computed cell volume change of anatase TiO_2 structure on the Al^{3+} ion content (x).

We then measured the electrochemical performance of TiO_2 NRs at a high current density of 0.5 A g^{-1}. **Figure 4a** shows the typical voltage profiles of the TiO_2 NRs. After the 20th cycle, the capacities of 40 mAh g^{-1} and 73 mAh g^{-1} in the mild and highly acidic chloroaluminate electrolyte were obtained, respectively. As follows from **Figure 4b**, for a 2.0 molar ratio, a high capacity retention of TiO_2 NRs was observed in comparison to the capacity retention with the 1.1 molar ratio. We note that the capacity difference measured in the mild and acidic solutions might be attributed to the difference in the Al^{3+} ion charge storage

mechanisms that are discussed in detail above. Lower coulombic efficiency being observed in chloroaluminate ionic liquid electrolyte with 2.0 : 1 molar ratio ($AlCl_3$:EMIMCl) as compared to that of slightly acidic liquid (1.1 : 1 molar ratio) can be explained by the enhanced corrosivity of the highly acidic melt with respect to the W current collector. Having established that the higher acidity of the electrolyte solution offers higher capacity, we studied the electrochemical performance of TiO_2 NRs in greater detail using a higher acidity electrolyte (**Figure 4c**, **d**). Namely, we revealed that the constant current-constant voltage (CCCV) charge at a constant voltage step of 1.2 V, improves the discharge capacity of TiO_2 NRs to 91 mAh g^{-1}. Notably, irreversibility between charge and discharge curves within first cycles (Figure 4d) might be associated with partial trapping of Al^{3+} ions in TiO_2 lattice. The cycling stability tests of half-cells employing TiO_2 NRs with a CCCV protocol at a current density of 0.5 A g^{-1} showed high capacity retention for 150 cycles with a Coulombic efficiency of ~99.9% (**Figure 4b**). TEM measurements of TiO_2 NRs after 150 cycles revealed that their structure and morphology was fully preserved (**Figure S13**). Importantly, TiO_2 NRs possess one of the most stable Al-ion cathodic performances with high capacity published to date for AIBs (for details see **Table S2**).

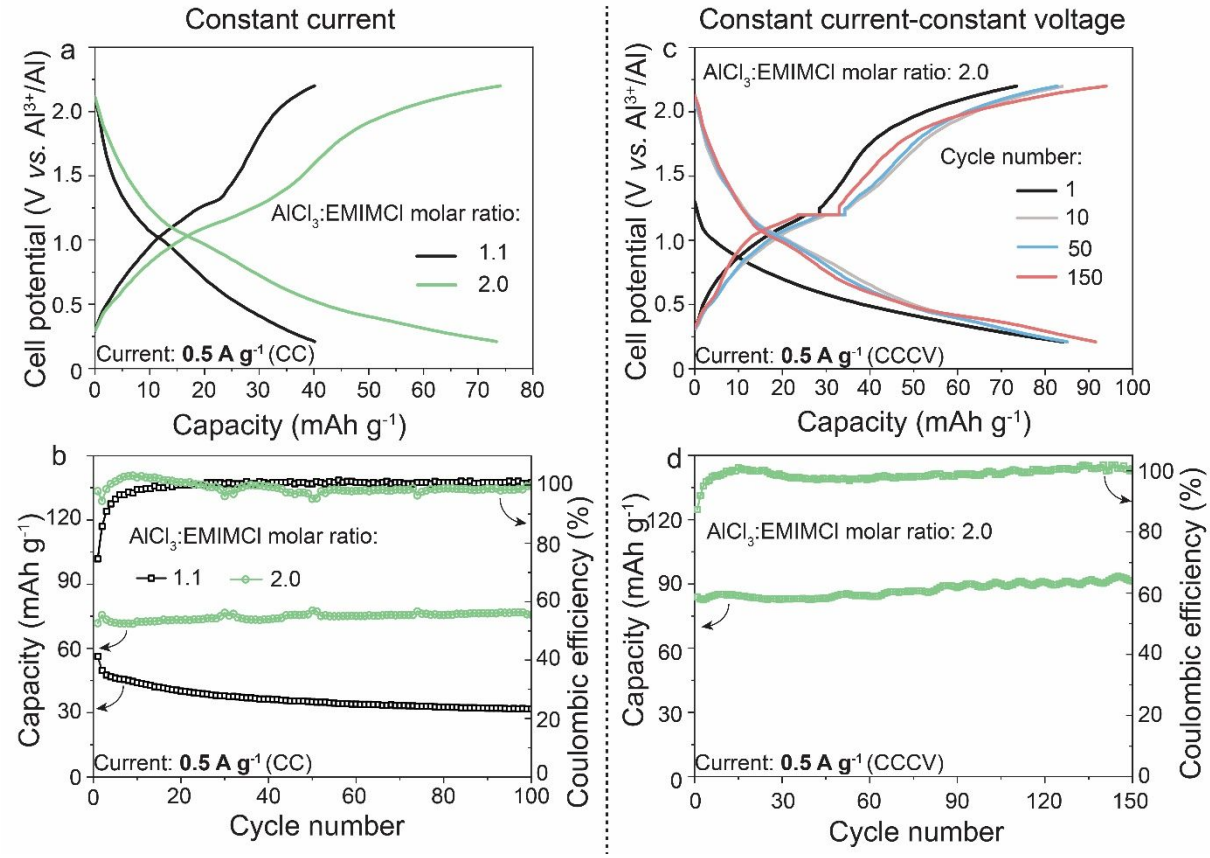

Figure 4. (a) Galvanostatic charge-discharge curves of TiO_2 NRs during the 20th cycle and (b) their cyclic stability measured at a current density of 0.5 A g^{-1} using $AlCl_3$:EMIMCl electrolytes (1.1:1 and 2.0:1 molar ratios). (c) Charge and discharge voltage profiles and (d) cyclic performance of TiO_2 NRs tested at current density of 0.5 A g^{-1} using CCCV mode (2:1 ($AlCl_3$/EMIMCl molar ratio). See also **Figure S14** for cyclic stability measurements of TiO_2 NRs at a current density of 50 mA g^{-1}.

CONCLUSIONS

In summary, we report the assessment of TiO_2 NRs as a cathode material for Al-ion storage. TiO_2 NRs exhibit high capacities of 112 mAh g^{-1} and 165 mAh g^{-1} at a current density of 50 mA g^{-1} in mild and highly acidic ($AlCl_3$/EMIMCl molar ratios of 1.1:1 and 2.0:1) chloroaluminate ionic liquid electrolytes, respectively. Moreover, TiO_2 NRs can be cycled at high current densities of 0.5 A g^{-1} (2.0:1 molar ratio), and they deliver a high capacity of approximately 90 mA g^{-1} without capacity fading over 150 cycles. The mechanism of Al^{3+} ion intercalation/deintercalation was probed by *ex situ* XPS and EDX measurements. The result evidence the electrochemical reduction/oxidation of Ti^{4+}/Ti^{3+} ions and insertion of Al^{3+} ions for both the 1.1:1 and 2.0:1 ratios during the discharging/charging of TiO_2 NRs.

Structural changes during Al^{3+} ion intercalation into an anatase TiO_2 structure were assessed by using DFT calculations which indicated the structural stability of the Al_xTiO_2 structure at a low Al^{3+} ion content of $x < 0.167$.

EXPERIMENTAL SECTION

Synthesis of TiO_2 NRs. Titanium oxide NRs were synthesized using a previously reported method. A volume of 6.9 mL of titanium isopropoxide (TIPO) was added to 6.7 mL of triethanolamine under stirring. Then, 16.4 mL of deionized water was added into the reaction mixture following the addition of 1.4 mL of ethylenediamine (in 15 min) under vigorous stirring. Afterward, the solution was brought to a total volume of 100 mL with water. The closed flask was heated to 100 °C for 24 h. The synthesized gel was transferred into autoclave for a second heat-treatment at 140 °C for 72 h. Lastly, as-synthesized TiO_2 NRs were collected from the autoclave and washed with water and HNO_3 (3 mol L^{-1}), following their centrifugation and drying under a dry air flow for 12h.

Electrochemical characterization of TiO_2 NRs. The following battery components/chemicals were used: carbon black (Super C65, TIMCAL), poly(vinylidene fluoride) (PVdF, Sigma-Aldrich), titanium nitride (TiN, 99.8%), N-methyl-2-pyrrolidone (NMP, 99%, Sigma-Aldrich), anhydrous $AlCl_3$ (99.99%, ABCR), 1-ethyl-3-methylimidazolium chloride (EMIMCl, 99%, Iolitec), W plate (Bocheng Molybdenum Co., Ltd), titanium (IV) oxide (anatase, 99.9%, Aldrich), Al foil (MTI Corporation), and glass microfiber separator (GF/D, Whatman). TiO_2 electrodes were prepared by mixing of TiO_2 NRs (45 wt. %), carbon black (CB, 22.5 wt. %), titanium nitride (TiN, 22.5 wt, %), and poly(vinylidene) fluoride binder (pVdF, 10 wt. %) using a Fritsch Pulverisette 7 classic planetary mill for 1 h at 500 rpm. The obtained homogeneous suspension was painted onto W current collectors following the drying step at 80 °C for 12 hours under vacuum (loading ~1

mg cm^{-2}). It is worth noting that, the contribution from empty W current collector to the capacity of TiO_2 electrodes prepared on W plates is negligible (see **Figure S15**).

Electrochemical measurements were conducted in homemade plastic cells (**Figure S3**), in an Ar-filled glove box (O_2 < 0.1 ppm, H_2O < 0.1 ppm) using glass fiber filter as a separator, and $AlCl_3$:EMIMCl ionic liquid as an electrolyte. Aluminum foil was used as both reference and counter electrodes. $AlCl_3$:EMIMCl ionic liquid (1.1:1 and 2:1 molar ratios) was used as the electrolyte. We note that highest molar ratio of $AlCl_3$:EMIMCl is ≈ 2 because above this ratio $AlCl_3$ can not be dissolved anymore in the choloroaluminate ionic liquid electrolyte.[8] Notably, in case of the use of chloroaluminate ionic liquid with molar ratio of 2:1, small corrosion of Al anode was observed as visible from SEM images of cycled Al foil (**Figure S16**). Electrochemical measurements were performed on an MPG2 multi-channel workstation (BioLogic) using a voltage range of 0.2-2.2 V *vs*. Al^{3+}/Al. For constant current-constant voltage (CCCV) measurements, constant voltage step was applied during charge at 1.2 V *vs.* Al^{3+}/Al. CCCV protocol at 1.2 V had been chosen mainly because it allowed to boost the discharge capacity of TiO_2 while having high coulombic efficiency during cycling. CV step at voltages of > 1.2 V significantly decreased the Coulombic efficiency. On the contrary, CV step at voltages of < 1.2 V had a limited contribution to the capacity. The charge storage capacity was normalized by the mass of TiO_2 NRs. Importantly, although TiO_2 electrodes were composed of TiN, pVdF and CB additives, the latter have a negligible contribution to the charge storage capacity of TiO_2 as indicated in **Figure S17**. TiN was used, as an additive, which helps to improve the electronic conductivity of TiO_2 electrodes.[61]

In order to understand whether brookite impurity has any impact on the electrochemical performance of anatase TiO_2 NRs, we have performed separately electrochemical measurements of TiO_2 brookite NPs (**Figure S18**). It has been revealed that bookite TiO_2 structure has lower electrochemical performance in comparison with anatase structure. TiO_2

brookite NPs have been synthesized following the procedure reported by Pottier *et al*.[62] (see **Figure S19** for XRD and TEM images).

Materials characterization. Scanning electron microscopy (SEM) of the as-obtained sample was done on a Quanta 200F microscope (Thermo Fisher Scientific) operated at an acceleration voltage Vacc = 20 kV. Energy-dispersive X-ray spectroscopy (EDXS) was performed with an Octane SDD detector (EDAX (Ametec)) attached to the microscope column. For spectra recording and quantification (ZAF correction), the software Gemini (EDAX) was used. The Powder X-ray diffraction (XRD) patterns were recorded using a Stoe & Cie Stadi P diffractometer in Debye-Scherrer setup, equipped with a focusing Ge-monochromator (Cu Kα1-radiation, λ = 1.54059 Å) and a Dectris Mythen 1K silicon strip detector. Solution NMR spectra were recorded using Bruker Advance 400 MHz spectrometer.

Rietveld Refinement of the Pristine TiO_2 (Anatase). A Rietveld refinement with GSAS II[63] was performed using the structural parameters of TiO_2 in the anatase structure.[64] A very small peak 30.72° (broad) is assigned to TiO_2 in the brookite structure (about 6.3 wt.%, crystallite size of 20 nm was assumed). The values for the lattice constants of TiO_2 (anatase) are a = 3.80002 (10) Å, c = 9.5010(2) Å, the cell volume is V = 137.20(1) $Å^3$. The values for the crystallite size were described with an "uniaxial" model, (anisotropic axis [0, 0, 1]) and refined to 0.012 and 0.029 μm, respectively.The figures of merit are Rp = 0.024, Rwp = 0.034, R(F)anatase = 0.028, R(F2)anatase = 0.045, $\chi 2$ = 8.679, GOOF = 2.946.

Computational Details. Calculations were carried out using periodic density functional theory (DFT) within the Vienna Ab initio Simulation Package (VASP).[65-66] The projected augmented wave (PAW) method was used to describe the inner cores and electron-ion interactions.[67-68] The exchange-correlation effects were treated by the Perdew-Burke-Ernzehof (PBE) functional with the generalized gradient approximation (GGA).[69] A supercell containing 108 atoms with 3×3×1 unit cells was modeled for TiO_2 anatase.[20, 70] To maximize computational efficiency without affecting the accuracy of the calculation, a plane wave cut-

off energy of 500 eV and the Monkhorst Pack grid of 5×5×2 were used in all calculations. The tetrahedron method with Blöchl corrections with a smearing width of σ = 0.05 eV was used to minimize the errors in the Hellmann-Feynman forces. Full relaxation of the supercell volume and atom positions was performed until the forces converged to less than 0.1 meV $Å^{-1}$. All structures were optimized with a convergence criterion of 0.01 meV for the energy calculation.

ASSOCIATED CONTENT

Supporting Information. Supporting Figures S1-S19 and Tables S1-S2. This material is available free of charge *via* the Internet at http://pubs.acs.org.

AUTHOR INFORMATION

Corresponding Authors:

*E-mail: mvkovalenko@ethz.ch

Author Contributions

The manuscript was written through the contributions of all authors. All authors have given approval to the final version of the manuscript.

ACKNOWLEDGMENTS

This research is part of the activities of SCCER HaE, which is financially supported by Innosuisse - Swiss Innovation Agency This work was also financially supported by the National Natural Science Foundation of China (Nos. 91834301 and 21878078). SPR, SC and OD greatly acknowledge the financial support of the synthesis work by the French

ANR within the Photonorm project (ANR-11-ECOT-0008). The authors are grateful to the research facilities of ETH Zürich (ETH Electron Microscopy Center, Department of Chemistry and Applied Biosciences) and Empa (Empa Electron Microscopy Center and Laboratory for Mechanics of Materials & Nanostructures) for access to the instruments and for technical assistance.

REFERENCES

(1) Hu, Y.; Sun, D.; Luo, B.; Wang, L. Recent Progress and Future Trends of Aluminum Batteries. *Energy Technology* **2019,** *7* (1), 86-106.
(2) Zhang, Y.; Liu, S.; Ji, Y.; Ma, J.; Yu, H. Emerging Nonaqueous Aluminum-Ion Batteries: Challenges, Status, and Perspectives. *Adv. Mater.* **2018,** *30* (38), 1706310.
(3) Wang, S. T.; Kravchyk, K. V.; Krumeich, F.; Kovalenko, M. V. Kish Graphite Flakes as a Cathode Material for an Aluminum Chloride-Graphite Battery. *ACS Appl. Mater. Interfaces* **2017,** *9* (34), 28478-28485.
(4) Chen, H.; Xu, H.; Wang, S.; Huang, T.; Xi, J.; Cai, S.; Guo, F.; Xu, Z.; Gao, W.; Gao, C. Ultrafast all-climate aluminum-graphene battery with quarter-million cycle life. *Sci. Adv.* **2017,** *3* (12), eaao7233.
(5) Stadie, N. P.; Wang, S. T.; Kravchyk, K. V.; Kovalenko, M. V. Zeolite-Templated Carbon as an Ordered Microporous Electrode for Aluminum Batteries. *ACS Nano* **2017,** *11* (2), 1911-1919.
(6) Walter, M.; Kravchyk, K. V.; Böfer, C.; Widmer, R.; Kovalenko, M. V. Polypyrenes as High-Performance Cathode Materials for Aluminum Batteries. *Adv. Mater.* **2018,** *30* (15), 1705644.
(7) Kravchyk, K. V.; Wang, S.; Piveteau, L.; Kovalenko, M. V. Efficient Aluminum Chloride Natural Graphite Battery. *Chem. Mater.* **2017,** *29* (10), 4484-4492.
(8) Kravchyk, K. V.; Kovalenko, M. V. Rechargeable Dual-Ion Batteries with Graphite as a Cathode: Key Challenges and Opportunities. *Adv. Energy Mater.* **2019,** 1901749.
(9) Levi, E.; Levi, M. D.; Chasid, O.; Aurbach, D. A Review on the Problems of the Solid State Ions Diffusion in Cathodes for Rechargeable Mg Batteries. *J. Electroceram.* **2009,** *22* (1), 13-19.
(10) Gu, S.; Wang, H.; Wu, C.; Bai, Y.; Li, H.; Wu, F. Confirming Reversible Al^{3+} Storage Mechanism Through Intercalation of Al^{3+} Into V_2O_5 Nanowires in a Rechargeable Aluminum Battery. *Energy Storage Mater.* **2017,** *6*, 9-17.
(11) Chiku, M.; Takeda, H.; Matsumura, S.; Higuchi, E.; Inoue, H. Amorphous Vanadium Oxide/Carbon Composite Positive Electrode for Rechargeable Aluminum Battery. *ACS Appl. Mater. Interfaces* **2015,** *7* (44), 24385-24389.
(12) Wang, H.; Bai, Y.; Chen, S.; Luo, X.; Wu, C.; Wu, F.; Lu, J.; Amine, K. Binder-Free V_2O_5 Cathode for Greener Rechargeable Aluminum Battery. *ACS Appl. Mater. Interfaces* **2015,** *7* (1), 80-84.
(13) Wang, W.; Jiang, B.; Xiong, W.; Sun, H.; Lin, Z.; Hu, L.; Tu, J.; Hou, J.; Zhu, H.; Jiao, S. A New Cathode Material for Super-Valent Battery Based on Aluminium Ion Intercalation and Deintercalation. *Sci. Rep.* **2013,** *3*, 3383.

(14) Wei, J.; Chen, W.; Chen, D.; Yang, K. Molybdenum Oxide as Cathode for High Voltage Rechargeable Aluminum Ion Battery. *J. Electrochem. Soc.* **2017,** *164* (12), A2304-A2309.
(15) Zhang, X. F.; Zhang, G. H.; Wang, S.; Li, S. J.; Jiao, S. Q. Porous CuO Microsphere Architectures as High-Performance Cathode Materials for Aluminum-Ion Batteries. *J. Mater. Chem. A* **2018,** *6* (7), 3084-3090.
(16) Liu, S.; Hu, J. J.; Yan, N. F.; Pan, G. L.; Li, G. R.; Gao, X. P. Aluminum Storage Behavior of Anatase TiO_2 Nanotube Arrays in Aqueous Solution for Aluminum Ion Batteries. *Energy Environ. Sci.* **2012,** *5* (12), 9743-9746.
(17) Liu, Y.; Sang, S.; Wu, Q.; Lu, Z.; Liu, K.; Liu, H. The Electrochemical Behavior of Cl^- Assisted Al^{3+} Insertion into Titanium Dioxide Nanotube Arrays in Aqueous Solution for Aluminum Ion Batteries. *Electrochim. Acta* **2014,** *143*, 340-346.
(18) Zhong, W.; Sang, S.; Liu, Y.; Wu, Q.; Liu, K.; Liu, H. Electrochemically Conductive Treatment of TiO_2 Nanotube Arrays in $AlCl_3$ Aqueous Solution for Supercapacitors. *J. Power Sources* **2015,** *294*, 216-222.
(19) Koketsu, T.; Ma, J.; Morgan, B. J.; Body, M.; Legein, C.; Dachraoui, W.; Giannini, M.; Demortiere, A.; Salanne, M.; Dardoize, F.; Groult, H.; Borkiewicz, O. J.; Chapman, K.; Strasser, P.; Dambournet, D. Reversible Magnesium and Aluminium Ions Insertion in Cation-Deficient Anatase TiO_2. *Nat. Mater.* **2017,** *16* (11), 1142.
(20) Tang, W. Q.; Xuan, J.; Wang, H. Z.; Zhao, S. L.; Liu, H. L. First-principles Investigation of Aluminum Intercalation and Diffusion in TiO_2 Materials: Anatase versus Rutile. *J. Power Sources* **2018,** *384*, 249-255.
(21) Sang, S.; Liu, Y.; Zhong, W.; Liu, K.; Liu, H.; Wu, Q. The electrochemical behavior of TiO_2-NTAs electrode in H^+ and Al^{3+} coexistent aqueous solution. *Electrochim. Acta* **2016,** *187*, 92-97.
(22) Lahan, H.; Boruah, R.; Hazarika, A.; Das, S. K. Anatase TiO_2 as an Anode Material for Rechargeable Aqueous Aluminum-Ion Batteries: Remarkable Graphene Induced Aluminum Ion Storage Phenomenon. *J. Phys. Chem. C* **2017,** *121* (47), 26241-26249.
(23) Geng, L. X.; Lv, G. C.; Xing, X. B.; Guo, J. C. Reversible Electrochemical Intercalation of Aluminum in Mo_6S_8. *Chem. Mater.* **2015,** *27* (14), 4926-4929.
(24) Hu, Y. X.; Ye, D. L.; Luo, B.; Hu, H.; Zhu, X. B.; Wang, S. C.; Li, L. L.; Peng, S. J.; Wang, L. Z. A Binder-Free and Free-Standing Cobalt Sulfide@Carbon Nanotube Cathode Material for Aluminum-Ion Batteries. *Adv. Mater.* **2018,** *30* (2), 1703824.
(25) Li, H.; Yang, H.; Sun, Z.; Shi, Y.; Cheng, H.-M.; Li, F. A Highly Reversible Co_3S_4 Microsphere Cathode Material for Aluminum-Ion Batteries. *Nano Energy* **2019,** *56*, 100-108.
(26) Wu, L.; Sun, R.; Xiong, F.; Pei, C.; Han, K.; Peng, C.; Fan, Y.; Yang, W.; An, Q.; Mai, L. A Rechargeable Aluminum-Ion Battery Based on a VS_2 Nanosheet Cathode. *Phys. Chem. Chem. Phys.* **2018,** *20* (35), 22563-22568.
(27) Zhang, X. F.; Wang, S.; Tu, J. G.; Zhang, G. H.; Li, S. J.; Tian, D. H.; Jiao, S. Q. Flower-like Vanadium Suflide/Reduced Graphene Oxide Composite: An Energy Storage Material for Aluminum-Ion Batteries. *Chemsuschem* **2018,** *11* (4), 709-715.
(28) Hu, Y. X.; Luo, B.; Ye, D. L.; Zhu, X. B.; Lyu, M. Q.; Wang, L. Z. An Innovative Freeze-Dried Reduced Graphene Oxide Supported SnS_2 Cathode Active Material for Aluminum-Ion Batteries. *Adv. Mater.* **2017,** *29* (48), 1606132.
(29) Liang, K.; Ju, L.; Koul, S.; Kushima, A.; Yang, Y. Self-Supported Tin Sulfide Porous Films for Flexible Aluminum-Ion Batteries. *Adv. Energy Mater.* **2018,** *9* (2), 1802543.
(30) Li, Z.; Niu, B.; Liu, J.; Li, J.; Kang, F. Rechargeable Aluminum-Ion Battery Based on MoS_2 Microsphere Cathode. *ACS Appl. Mater. Interfaces* **2018,** *10* (11), 9451-9459.
(31) Takami, N.; Koura, N. Studies on the Electrochemical Behaviour of the FeS_2 Electrode in Molten $AlCl_3$·NaCl by the AC Impedance Method. *Electrochim. Acta* **1988,** *33* (1), 69-74.
(32) Wang, S.; Yu, Z.; Tu, J.; Wang, J.; Tian, D.; Liu, Y.; Jiao, S. A Novel Aluminum-Ion Battery: Al/$AlCl_3$-EMImCl/Ni_3S_2@Graphene. *Adv. Energy Mater.* **2016,** *6* (13), 1600137.

(33) Yu, Z.; Kang, Z.; Hu, Z.; Lu, J.; Zhou, Z.; Jiao, S. Hexagonal NiS Nanobelts as Advanced Cathode Materials for Rechargeable Al-Ion Batteries. *Chem. Commun.* **2016,** *52* (68), 10427-10430.
(34) Geng, L. X.; Scheifers, J. P.; Fu, C. Y.; Zhang, J.; Fokwa, B. P. T.; Guo, J. C. Titanium Sulfides as Intercalation-Type Cathode Materials for Rechargeable Aluminum Batteries. *ACS Appl. Mater. Interfaces* **2017,** *9* (25), 21251-21257.
(35) Kulish, V. V.; Koch, D.; Manzhos, S. Aluminium and Magnesium Insertion in Sulfur-Based Spinels: a First-Principles Study. *Phys. Chem. Chem. Phys.* **2017,** *19* (8), 6076-6081.
(36) Wang, S.; Jiao, S.; Wang, J.; Chen, H.-S.; Tian, D.; Lei, H.; Fang, D.-N. High-Performance Aluminum-Ion Battery with CuS@C Microsphere Composite Cathode. *Acs Nano* **2017,** *11* (1), 469-477.
(37) Cai, T.; Zhao, L.; Hu, H.; Li, T.; Li, X.; Guo, S.; Li, Y.; Xue, Q.; Xing, W.; Yan, Z.; Wang, L. Stable $CoSe_2$/Carbon Nanodice@reduced Graphene Oxide Composites for High-Performance Rechargeable Aluminum-Ion Batteries. *Energy Environ. Sci.* **2018,** *11* (9), 2341-2347.
(38) Jiang, J.; Li, H.; Fu, T.; Hwang, B.-J.; Li, X.; Zhao, J. One-Dimensional $Cu_{2-x}Se$ Nanorods as the Cathode Material for High-Performance Aluminum-Ion Battery. *ACS Appl. Mater. Interfaces* **2018,** *10* (21), 17942-17949.
(39) Tu, J.; Lei, H.; Wang, M.; Yu, Z.; Jiao, S. Facile Synthesis of $Ni_{11}(HPO_3)_8(OH)_6$/rGO Nanorods with Enhanced Electrochemical Performance for Aluminum-Ion Batteries. *Nanoscale* **2018,** *10* (45), 21284-21291.
(40) Nacimiento, F.; Cabello, M.; Alcántara, R.; Pérez-Vicente, C.; Lavela, P.; Tirado, J. L. Exploring an Aluminum Ion Battery Based on Molybdite as Working Electrode and Ionic Liquid as Electrolyte. *J. Electrochem. Soc.* **2018,** *165* (13), A2994-A2999.
(41) Jiang, J.; Li, H.; Huang, J.; Li, K.; Zeng, J.; Yang, Y.; Li, J.; Wang, Y.; Wang, J.; Zhao, J. Investigation of the Reversible Intercalation/Deintercalation of Al into the Novel Li_3VO_4@C Microsphere Composite Cathode Material for Aluminum-Ion Batteries. *ACS Appl. Mater. Interfaces* **2017,** *9* (34), 28486-28494.
(42) VahidMohammadi, A.; Hadjikhani, A.; Shahbazmohamadi, S.; Beidaghi, M. Two-Dimensional Vanadium Carbide (MXene) as a High-Capacity Cathode Material for Rechargeable Aluminum Batteries. *Acs Nano* **2017,** *11* (11), 11135-11144.
(43) Reed, L. D.; Ortiz, S. N.; Xiong, M.; Menke, E. J. A Rechargeable Aluminum-Ion Battery Utilizing a Copper Hexacyanoferrate Cathode in an Organic Electrolyte. *Chem. Commun.* **2015,** *51* (76), 14397-14400.
(44) Liu, S.; Pan, G. L.; Li, G. R.; Gao, X. P. Copper Hexacyanoferrate Nanoparticles as Cathode Material for Aqueous Al-Ion Batteries. *J. Mater. Chem. A* **2015,** *3* (3), 959-962.
(45) Zhang, S.; Tan, X.; Meng, Z.; Tian, H.; Xu, F.; Han, W.-Q. Naturally Abundant High-Performance Rechargeable Aluminum/Iodine Batteries Based on Conversion Reaction Chemistry. *J. Mater. Chem. A* **2018,** *6* (21), 9984-9996.
(46) Huang, X.; Liu, Y.; Liu, C.; Zhang, J.; Noonan, O.; Yu, C. Rechargeable Aluminum–Selenium Batteries With High Capacity. *Chem. Sci.* **2018,** *9* (23), 5178-5182.
(47) Yang, H.; Yin, L.; Liang, J.; Sun, Z.; Wang, Y.; Li, H.; He, K.; Ma, L.; Peng, Z.; Qiu, S.; Sun, C.; Cheng, H.-M.; Li, F. An Aluminum–Sulfur Battery with a Fast Kinetic Response. *Angew. Chem., Int. Ed.* **2018,** *57* (7), 1898-1902.
(48) Bian, Y.; Li, Y.; Yu, Z.; Chen, H.; Du, K.; Qiu, C.; Zhang, G.; Lv, Z.; Lin, M.-C. Using an $AlCl_3$/Urea Ionic Liquid Analog Electrolyte for Improving the Lifetime of Aluminum-Sulfur Batteries. *ChemElectroChem* **2018,** *5*, 3607-3611.
(49) Cohn, G.; Ma, L.; Archer, L. A. A Novel Non-Aqueous Aluminum Sulfur Battery. *J. Power Sources* **2015,** *283*, 416-422.

(50) Wang, L.; Liu, F.; Wang, W.; Yang, G.; Zheng, D.; Wu, Z.; Leung, M. K. H. A High-Capacity Dual-Electrolyte Aluminum/air Electrochemical Cell. *RSC Advances* **2014,** *4* (58), 30857-30863.
(51) Kazazi, M.; Abdollahi, P.; Mirzaei-Moghadam, M. High Surface Area TiO_2 Nanospheres as a High-Rate Anode Material for Aqueous Aluminium-Ion Batteries. *Solid State Ionics* **2017,** *300*, 32-37.
(52) He, Y. J.; Peng, J. F.; Chu, W.; Li, Y. Z.; Tong, D. G. Black Mesoporous Anatase TiO_2 Nanoleaves: a High Capacity and High Rate Anode for Aqueous Al-Ion Batteries. *J. Mater. Chem. A* **2014,** *2* (6), 1721-1731.
(53) Das, S. K.; Palaniselvam, T.; Adelhelm, P. Electrochemical Study on the Rechargeability of TiO_2 as Electrode Material for Al-ion Batteries with Chloroaluminate Ionic Liquid Electrolyte. *Solid State Ionics* **2019,** *340*, 115017.
(54) Dufour, F.; Pigeot-Remy, S.; Durupthy, O.; Cassaignon, S.; Ruaux, V.; Torelli, S.; Mariey, L.; Maugé, F.; Chanéac, C. Morphological Control of TiO_2 Anatase Nanoparticles: What Is the Good Surface Property to Obtain Efficient Photocatalysts? *Appl. Catal., B* **2015,** *174-175*, 350-360.
(55) Sugimoto, T.; Zhou, X.; Muramatsu, A. Synthesis of Uniform Anatase TiO_2 Nanoparticles by Gel–Sol Method: 3. Formation Process and Size Control. *J. Colloid Interface Sci.* **2003,** *259* (1), 43-52.
(56) Tsuda, T.; Stafford, G. R.; Hussey, C. L. Review-Electrochemical Surface Finishing and Energy Storage Technology with Room-Temperature Haloaluminate Ionic Liquids and Mixtures. *J. Electrochem. Soc.* **2017,** *164* (8), H5007-H5017.
(57) Abood, H. M. A.; Abbott, A. P.; Ballantyne, A. D.; Ryder, K. S. Do All Ionic Liquids Need Organic Cations? Characterisation of $[AlCl_2 \cdot nAmide]^+AlCl_4^-$ and Comparison with Imidazolium Based Systems. *Chem. Commun.* **2011,** *47* (12), 3523-3525.
(58) Angell, M.; Pan, C. J.; Rong, Y. M.; Yuan, C. Z.; Lin, M. C.; Hwang, B. J.; Dai, H. J. High Coulombic Efficiency Aluminum-Ion Battery Using an $AlCl_3$-Urea Ionic Liquid Analog Electrolyte. *Proc. Natl. Acad. Sci. U. S. A.* **2017,** *114* (5), 834-839.
(59) Noth, H.; Rurlander, R.; Wolfgardt, P. An Investigation of $AlCl_3$ Solutions in Ethers by ^{27}Al NMR Spectroscopy. *Z. Naturforsch. B Chem. Sci.* **1982,** *37* (1), 29-37.
(60) Kim, D. J.; Yoo, D.-J.; Otley, M. T.; Prokofjevs, A.; Pezzato, C.; Owczarek, M.; Lee, S. J.; Choi, J. W.; Stoddart, J. F. Rechargeable aluminium organic batteries. *Nat. Energy* **2019,** *4*, 51-59.
(61) Wang, S.; Kravchyk, K. V.; Filippin, A. N.; Müller, U.; Tiwari, A. N.; Buecheler, S.; Bodnarchuk, M. I.; Kovalenko, M. V. Aluminum Chloride-Graphite Batteries with Flexible Current Collectors Prepared from Earth-Abundant Elements. *Adv. Sci.* **2018,** *5* (4), 1700712.
(62) Pottier, A.; Chanéac, C.; Tronc, E.; Mazerolles, L.; Jolivet, J.-P. Synthesis of Brookite TiO_2 Nanoparticles by Thermolysis of $TiCl_4$ in Strongly Acidic Aqueous Media. *J. Mater. Chem.* **2001,** *11* (4), 1116-1121.
(63) Toby, B. H.; Von Dreele, R. B. GSAS-II: the Genesis of a Modern Open-source All Purpose Crystallography Software Package. *J. Appl. Crystallogr* **2013,** *46* (2), 544-549.
(64) Ballirano, P.; Caminiti, R. Rietveld Refinements on Laboratory Energy Dispersive X-ray Diffraction (EDXD) data. *J. Appl. Crystallogr* **2001,** *34* (6), 757-762.
(65) Kresse, G.; Hafner, J. Ab Initio Molecular Dynamics for Liquid Metals. *Phys. Rev. B* **1993,** *47* (1), 558-561.
(66) Kresse, G.; Furthmüller, J. Efficient Iterative Schemes for ab Initio Total-energy Calculations Using a Plane-Wave Basis Set. *Phys. Rev. B* **1996,** *54* (16), 11169-11186.
(67) Blöchl, P. E. Projector Augmented-wave Method. *Phys. Rev. B* **1994,** *50* (24), 17953-17979.
(68) Kresse, G.; Joubert, D. From Ultrasoft Pseudopotentials to the Projector Augmented-Wave Method. *Phys. Rev. B* **1999,** *59* (3), 1758-1775.

(69) Zhang, Y.; Yang, W. Comment on ``Generalized Gradient Approximation Made Simple". *Phys. Rev. Lett.* **1998,** *80* (4), 890-890.
(70) Dawson, J. A.; Robertson, J. Improved Calculation of Li and Na Intercalation Properties in Anatase, Rutile, and TiO_2(B). *J. Phys. Chem. C* **2016,** *120* (40), 22910-22917.

TABLE OF CONTENTS: